INORGANIC CHEMISTRY FRONTIERS

RESEARCH ARTICLE

View Article Online
View Journal | View Issue

Cite this: *Inorg. Chem. Front.*, 2024, **11**, 7872

Al-alkyl borate salt cocatalysts for olefin polymerization: exploration of N-donor ligand variations†

Gaia Urciuoli, [a,b,c] Francesco Zaccaria, *[a,c] Cristiano Zuccaccia, *[b,c] Roberta Cipullo, *[a,c] Peter H. M. Budzelaar, [a] Leonardo Tensi, [d] Antonio Vittoria, [a] Christian Ehm, [a,c] Alceo Macchioni [b,c] and Vincenzo Busico [a,c]

The well-defined Al-alkyl borate (AAB) salt $\{[iBu_2(PhNMe_2)Al]_2(\mu\text{-}H)\}^+[B(C_6F_5)_4]^-$ (**AlHAl**) has been recently identified as a promising "complete" cocatalyst for olefin polymerization. Herein, we explore structural variations of **AlHAl** obtained by replacing the $PhNMe_2$ (**DMA**) donor with a variety of anilines, amines, and N-heterocycles. Of the 18 investigated N-donors, twelve provided stable AAB salts; these were tested as cocatalysts in ethylene/1-hexene copolymerization with an archetypical metallocene catalyst. In the other six cases, the side reactions were thoroughly analyzed by NMR spectroscopy. For instance, addition of an *o*-Me substituent on the **DMA** ligand triggers C–H activation leading to five-membered cyclometalated species; increasing the steric bulk directly at the N-donor atom leads to tricoordinate mononuclear Al-alkyl cations, which could be isolated, fully characterized and tested in polymerization when using $PhNEt_2$ (**DEA**). The cocatalytic performance of aniline- and amine-based systems varies only marginally with respect to the benchmark **AlHAl_DMA**. N-heterocyclic AAB salts perform worse; only the two least electron donating donors, namely difluoropyridine (**Py-3,5-F**) and quinoline (**QUI**), provide noticeable productivity. A simple quantitative structure–activity relationship, correlating the steric bulk and stabilizing ability of the N-donor with productivity (R^2 = 0.88), has been identified.

Received 26th July 2024,
Accepted 14th September 2024

DOI: 10.1039/d4qi01874e

rsc.li/frontiers-inorganic

Introduction

Molecular olefin polymerization catalysis has tremendously progressed over the last few decades. Initially considered of mere academic interest, nowadays it is of great industrial relevance for the production of several, added-value polyolefin grades.[1] The key to success has been the identification of suitable precatalyst/cocatalyst combinations providing highly productive, selective and thermally stable catalytic systems.[2,3] Despite the comparable importance of a precatalyst and cocatalyst, these two components have evolved at very different paces. The design of ancillary ligand frameworks has been prolific and continues to provide novel high-performing group 4 metallocene and "post-metallocene" catalysts.[4,5] In contrast, diversification among cocatalysts is far more limited; the currently most widely used systems are still based on methylaluminoxane (MAO), discovered in the late 1970s,[6,7] or binary systems comprising of an aluminum trialkyl (*e.g.* tri-iso-butylaluminum, TIBAL) and a borate salt of organic Lewis or Brønsted acids (*e.g.* $[Ph_3C]^+$ $[B(C_6F_5)_4]^-$, trityl borate, TTB; $[PhMe_2NH]^+$ $[B(C_6F_5)_4]^-$, anilinium borate, AB), discovered in the 1990s.[8,9]

This discrepancy is due to the complexity of innovating cocatalysts to overcome their main drawbacks.[10–19] In the case of MAO, some of the most widely explored optimization strategies include replacing methyl with larger alkyl groups to improve stability and solubility,[20–22] and/or using additives like phenols,[23–25] $AlMe_2F$[26,27] or Lewis bases[28–30] to modulate reactivity. However, despite recent advancement,[31] the complex and poorly understood structure of this alumoxane hampered rational design and limited optimization, for instance, with respect to minimizing the high Al/M ratios

[a]*Department of Chemical Sciences, Federico II University of Naples, via Cinthia, 80126 Napoli, Italy. E-mail: francesco.zaccaria@unina.it, rcipullo@unina.it*
[b]*Department of Chemistry, Biology and Biotechnology, University of Perugia and CIRCC, via Elce di Sotto 8, 06123 Perugia, Italy.*
E-mail: cristiano.zuccaccia@unipg.it
[c]*DPI, P.O. Box 902, 5600 AX Eindhoven, the Netherlands*
[d]*Department of Pharmaceutical Sciences, University of Perugia, Via del Liceo 1, 06123 Perugia, Italy*

†Electronic supplementary information (ESI) available: Additional synthetic, characterization and computational details. CCDC 2372888–2372892. For ESI and crystallographic data in CIF or other electronic format see DOI: https://doi.org/10.1039/d4qi01874e

necessary for optimal performance (typically on the order of 10^3–10^4; M = group 4 metal).[7,15] The well-defined structure of borate salts allows fine tuning of both cation and anion properties,[3,8–19] but, also in this case, some main limitations remain like their ability to serve only as alkyl abstractors. This is the reason why an alkylating and scavenging agent like TIBAL is required with these borate activators, while MAO functions as a stand-alone and "complete" cocatalyst.

Recently, our group identified a borate salt containing an unusual homodinuclear Al-alkyl cation stabilized by *N*,*N*-dimethylaniline (**DMA**) ligands and a bridging hydride, namely $\{[iBu_2(PhNMe_2)Al]_2(\mu\text{-}H)\}^+[B(C_6F_5)_4]^-$ (**AlHAl**, Fig. 1a).[32] The coordinately saturated nature of the metal centers makes this Al-alkyl cation relatively easy to synthesize and stable at room temperature under an inert atmosphere, even though it still manifests a marked "latent"[33] Lewis acidity. In fact, propene polymerization experiments revealed that this species is a competent cocatalyst for typical group 4 metal based metallocenes and "post-metallocenes", exhibiting performance comparable to that of established cocatalysts like MAO and borate salts/TIBAL.[32,34]

The cocatalytic properties of this novel system are intriguing in several respects. First, like MAO, **AlHAl** is a "complete" cocatalyst, effectively activating both dimethyl and dichloride precatalysts and serving as an impurity scavenger. Notably, productivities comparable to those obtained with established cocatalysts, at the same catalyst concentration, can be achieved at Al/M ratios of a few tens, which is orders of magnitude lower than those typically needed with organic borate salts/TIBAL (10^2–10^3) or MAO (10^3–10^4).

Another important feature of **AlHAl** is its well-defined molecular structure. Recently, we reported a first proof-of-concept regarding the possibility to tune the properties of **AlHAl**: introduction of long alkyl chains on the **DMA** ligands allows overcoming one of the main limitations of ionic cocatalysts, that is their very low solubility in the saturated hydrocarbon diluents typically used in industrial solution processes.[35] This modified, soluble cocatalyst (**s-AlHAl** in Fig. 1b) could be employed successfully in combination with a representative zirconocene in ethylene/1-hexene copolymerization at 100 °C in an alkane diluent, providing a catalytic performance comparable to those of established cocatalysts adapted for the same purpose.

Herein, we report a broader study on the structural modification of **AlHAl**, aiming at expanding this family of well-defined Al-alkyl borate (AAB) salt cocatalysts. In particular, we explored the possibility of replacing the **DMA** ligands with a variety of other N-donors (**AlHAl_L**, Fig. 1c) and evaluated the effect of structural modifications on the properties of these systems by spectroscopic, polymerization and computational studies.

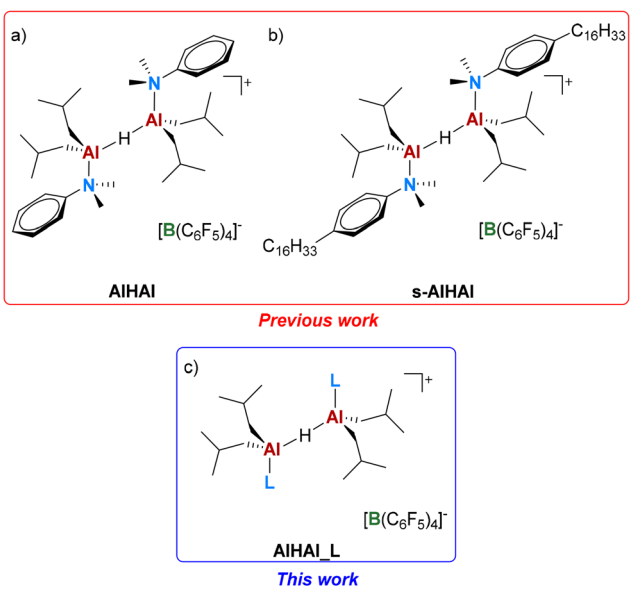

Fig. 1 Structure of **AlHAl**-type cocatalysts: (a) prototype,[32] (b) hydrocarbon soluble analogue,[35] and (c) structural variations explored herein (L = neutral N-donor, see Fig. 2).

Results and discussion

Synthesis and characterization

The 18 N-donors (**L**; Fig. 2) studied were selected from commercially available compounds to explore steric and electronic properties over three classes of molecules, namely anilines, amines, and N-heterocycles. Initially, the synthetic approach previously optimized for **AlHAl_DMA** was utilized (Scheme 1).[32,35] The reaction of equimolar amounts of TIBAL, N-donor and the borate salt of the protonated N-donor provides the mononuclear intermediate **Al_L**; iso-butane is the only (gaseous) byproduct. **Al_L** is subsequently converted into dinuclear **AlHAl_L** by addition of 1 eq. of di-iso-butylaluminum hydride (DIBAL-H; Scheme 1a); the mono- and dinuclear species are in dynamic equilibrium,[32] as further discussed in the following sections. Alternatively, the same **Al_L** intermediate can be obtained by reaction of TIBAL with two equivalents of N-donor and one equivalent of TTB (Scheme 1b). Although

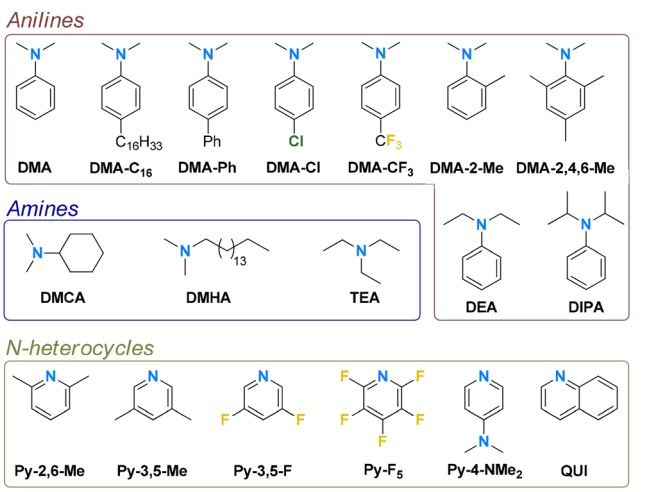

Fig. 2 N-donor ligands studied (**L**).

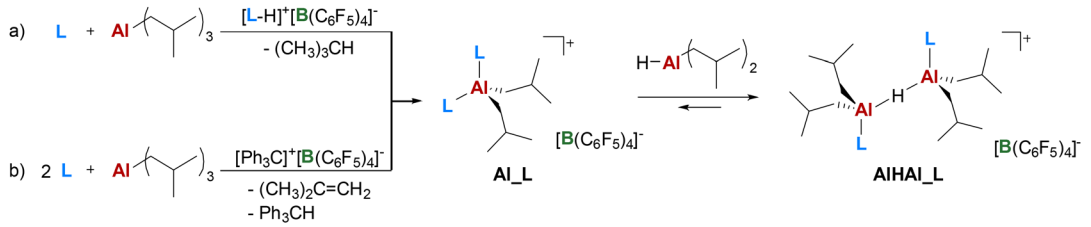

Scheme 1 Synthetic procedures explored for **AlHAl_L**, inspired by those previously optimized for **AlHAl_DMA**.[32] DIBAL-H is shown as a monomer for simplicity.

this approach is less atom-efficient, producing two byproducts, iso-butene and triphenylmethane, it can be employed for N-donors where the borate salt is not commercially available or easily synthesizable. Pure **Al_L** is then obtained by removing iso-butene *in vacuo* and triphenylmethane by washing with pentane. Both these approaches were employed depending on the specific properties of each N-donor.

Anilines and amines: successful attempts. Along with previously reported **DMA**[32] and **DMA-C$_{16}$**,[35] the synthetic protocols depicted in Scheme 1 were successfully applied to **DMA-Ph**, **DMA-Cl**, **DMCA** and **DMHA**. Since the anilinium/ammonium salts of these latter species are not commercially available, the synthetic protocol using TTB (Scheme 1b) was used in most cases. Only for **DMHA**, synthesizing the ammonium salt[36] and following the route of Scheme 1a is indicated; the long hexadecyl chain of this amine renders **Al_DMHA** highly soluble in pentane, precluding efficient removal of the Ph_3CH byproduct (route b).

Characterization of reaction products by NMR spectroscopy indicates that the structural properties of **AlHAl_L** are only marginally affected by donor variation (see the ESI for details†). The NMR spectra of the representative **AlHAl_DMA-Ph** are very similar to those reported previously for **AlHAl_DMA**,[32] the main difference being the additional signals due to the *p*-phenyl substituents (Fig. S37†).

Quantitative ^{1}H NMR analysis of equilibrium constants (K_{eq}) and corresponding Gibbs free energies (ΔG) for the reaction:

$$\mathbf{Al\_L} + [Al\mathit{i}Bu_2H]_3 \rightleftarrows \mathbf{AlHAl\_L} + [Al\mathit{i}Bu_2H]_2 \quad (1)$$

also indicates only a small effect of N-donor variation on the relative stability of the mono and dinuclear species at 298 K for **L** = anilines (entries 1–5, Table 1). As previously reported for the prototypical **DMA** system,[32] the dinuclear species is more stable, and solutions containing up to 90 mol% **AlHAl_L** can be prepared by properly dosing DIBAL-H (see the ESI†). For **L** = amines, a similar K_{eq} is observed with **DMHA** (entry 7, Table 1), even though the reaction between **Al_DMHA** and DIBAL-H is not instantaneous and requires approximately 12 h to equilibrate even in the presence of excess DIBAL-H (Fig. S12†); at these long reaction times, some decomposition products become detectable in the NMR spectra. In the case of **DMCA**, no reagents could be detected by NMR spectroscopy,

Table 1 Equilibrium constants (K_{eq}) and corresponding Gibbs free energy differences (ΔG) for the reaction reported in eqn (1) [a]

Entry	L	Solvent	K_{eq}	ΔG (kcal mol^{-1})	Ref.
1	**DMA**	C_7D_8	12	−1.5	32
2	**DMA**	C_6D_5Cl	12	−1.5	[d]
3	**DMA-C$_{16}$**	C_7D_8	23	−1.9	35
4	**DMA-Ph**	C_7D_8	11	−1.4	[d]
5	**DMA-Cl**	C_6D_5Cl	11	−1.4	[d]
6	**DMCA**	C_6D_5Cl	>23[c]	<−1.9	[d]
7	**DMHA**[b]	C_7D_8	13	−1.5	[d]
8	N-Heterocycles	C_7D_8	≪1[c]	≫0	[d]

[a] By quantitative ^{1}H NMR spectroscopy at 298 K. [b] Limited stability (see main text). [c] No accurate absolute values could be determined as the concentration of some relevant species is below detection limits of NMR. C_7D_8 = toluene-d_8, C_6D_5Cl = chlorobenzene-d_5. [d] This work.

suggesting nearly quantitative conversion to the dinuclear product (*i.e.* K_{eq} > 23; entry 6, Table 1).

Despite considerable efforts, no single crystals suitable for X-ray diffraction could be obtained for **AlHAl_L** as they precipitate as oils in all cases. The crystal structure could be instead analyzed for mononuclear **Al_L** with **L** = **DMA** and **DMA-Cl** (Fig. 3a and b). Both species exhibit the expected *pseudo*-tetrahedral geometry for tetracoordinated Al-complexes, with similar Al–C and Al–N bond lengths (entries 1 and 2, Table 2). The N–Al–N bond angles of ∼106° for **Al_DMA** and ∼104° for **Al_DMA-Cl** are close to the 109° angle of ideal tetrahedral geometry, while C–Al–C angles are appreciably higher (>120° in both cases; entries 1 and 2, Table 2) likely due to the steric constrain imparted by the bulky iso-butyl groups. Consistently, the C–Al–C angle reported for the methyl analogue of **Al_DMA**, *i.e.* $[AlMe_2(PhNMe_2)]^+[B(C_6F_5)_4]^-$, is appreciably smaller and is approximately 115°.[37]

Anilines and amines: side reactions. Side reactions hampered isolation or even detection of **Al_L** and **AlHAl_L** with the other anilines and amines. For instance, the *para*-substituted aniline **DMA_CF$_3$** undergoes C–F bond activation (Scheme 2a), which is known to potentially occur in the presence of Al-based Lewis acids.[38,39]

Conversely, with the *o*-Me substituted aniline, **Al_DMA-2-Me** could be obtained and characterized, even though it is unstable at 298 K and converted quantitatively within a few hours into the neutral cyclometalated species **Al_Cyclo1** and the **DMA-2-Me** anilinium borate salt (Scheme 2b). The identity

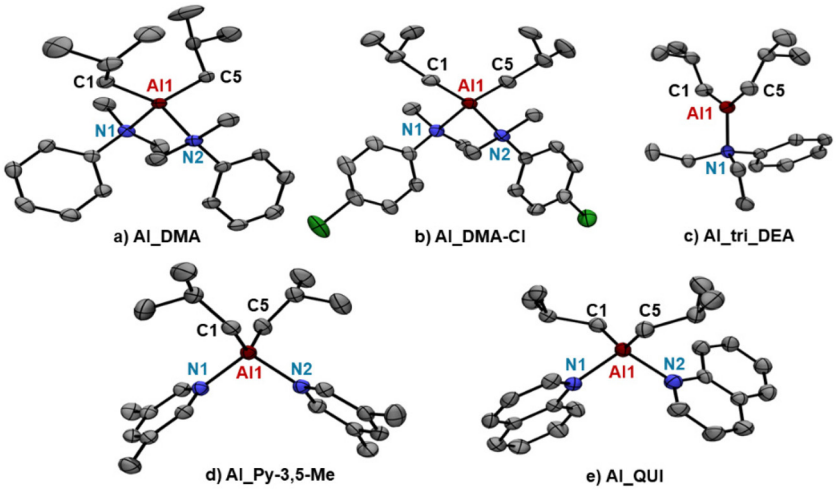

Fig. 3 Ortep drawings of (a) **Al_DMA**, (b) **Al_DMC-Cl**, (c) **Al_tri_DEA**, (d) **Al_Py-3,5-Me** and (e) **Al_QUI** crystal structures obtained by single crystal X-ray diffraction. Ellipsoids are drawn at 50% probability level. Hydrogen atoms, $[B(C_6F_5)_4]^-$ anion and solvent molecules are omitted for clarity. For further details, including relevant distances (Å) and angles (°), see Table 2 and the ESI.†

Table 2 Relevant distances (Å) and angles (°) for the crystal structure of **Al_L** salts reported in Fig. 3

Entry	Al_L	Al–C1	Al–C5	Al–N1	Al–N2	N–Al–N	C–Al–C
1	**Al_DMA**	1.9760(16)	1.9733(16)	2.0660(13)	2.0877(14)	106.22(5)	124.39(7)
2	**Al_DMA-Cl**	1.974(3)	1.982(4)	2.075(2)	2.080(3)	104.31(11)	122.39(15)
3	**Al_tri_DEA**	1.9393(16)	1.9421(16)	1.9766(14)	—	—	131.21(8)
4	**Al_Py-3,5-Me**	1.962(2)	1.968(2)	1.9758(19)	1.9703(19)	96.42(8)	121.91(11)
5	**Al_QUI**	1.958(3)	1.966(3)	2.001(3)	2.000(3)	99.53(11)	126.24(15)

of **Al_Cyclo1** was further confirmed by its independent synthesis *via* the sequential reaction of **DMA-2-Me** with BuLi and di-iso-butylaluminum chloride (DIBAL-Cl; Fig. S27†).[40,41] The decomposition of **Al_DMA-2-Me** is likely triggered by the steric hindrance imparted by the *o*-Me groups of the two aniline ligands. The reaction is reminiscent of directing group enabled C–H activation[42] with the hydrogen being transferred to the released base. It is worth noting that, even though Al–alkyl bonds are generally more reactive than Al–aniline ones, C–H activation leading to the cyclometalated species involves only the latter (Scheme 2b); somewhat related observations have been reported for $(BHT)_2AlMe$ (BHT = 2,6-di-*tert*-butyl-4-methylphenolate), in which the first Al–O bond is hydrolyzed more easily than the Al–Me one, likely due to the steric strain imparted by the bulky phenolate ligands.[43]

The reactivity of isolated **Al_Cyclo1** was preliminarily explored by reaction with TTB in the absence and presence of 1 equiv. of **DMA-2-Me**. In the former case, ionization and rapid (C_6F_5)-group abstraction from the borate anion are observed (Scheme S1†). In the latter, the reaction provides stable ionic **Al_Cyclo1_DMA-2-Me** (Scheme 2c), in which the Al center binds two aniline-type fragments and two alkyl groups analogously to **Al_DMA-2-Me**. Addition of DIBAL-H resulted in a complex and dynamic mixture of unknown products; evidence for complete conversion of *o*-Me groups into formally anionic methylene moieties was obtained after >24 h (Fig. S30†). Given the complexity of this reactivity and the rather low isolated yields, we decided not to further investigate these species.

With the even bulkier **DMA-2,4,6-Me**, having two *o*-Me and one *p*-Me groups, **Al_DMA-2,4,6-Me** could not be detected by NMR spectroscopy. Decomposition to the cyclometalated **Al_Cyclo2**, the borate salt of the donor, and a tricoordinate Al-alkyl cation having a single aniline coordinated to aluminum (**Al_tri_DMA-2,4,6-Me**, Scheme 2d) was observed. The latter species decomposes slowly to the cyclometalated complex, anilinium borate and a variety of other unknown products.

The clean formation of a tricoordinate species is instead observed with **DEA** (Scheme 2e), in which steric bulk is increased directly on the aniline N-donor atom and no easy routes to stable 5-membered cyclometalated species are accessible. **Al_tri_DEA** is stable in the solid form for weeks and decomposes only very slowly in solution over several days *via* (C_6F_5)-abstraction (Scheme S2†); it could be therefore thoroughly characterized by NMR spectroscopy and single-crystal X-ray diffraction, showing a nearly planar coordination geometry (Fig. 3c). **Al_tri_DEA** is one of the very few examples of stable and fully characterized tricoordinate Al-alkyl cations.[44–50] No reaction is observed upon adding DIBAL-H to **Al_tri_DEA** neither in the absence nor presence of an additional **DEA** equivalent.

The bulkier donor **DIPA** leads to a detectable but less stable tricoordinate complex **Al_tri_DIPA** (Scheme 2f), which decom-

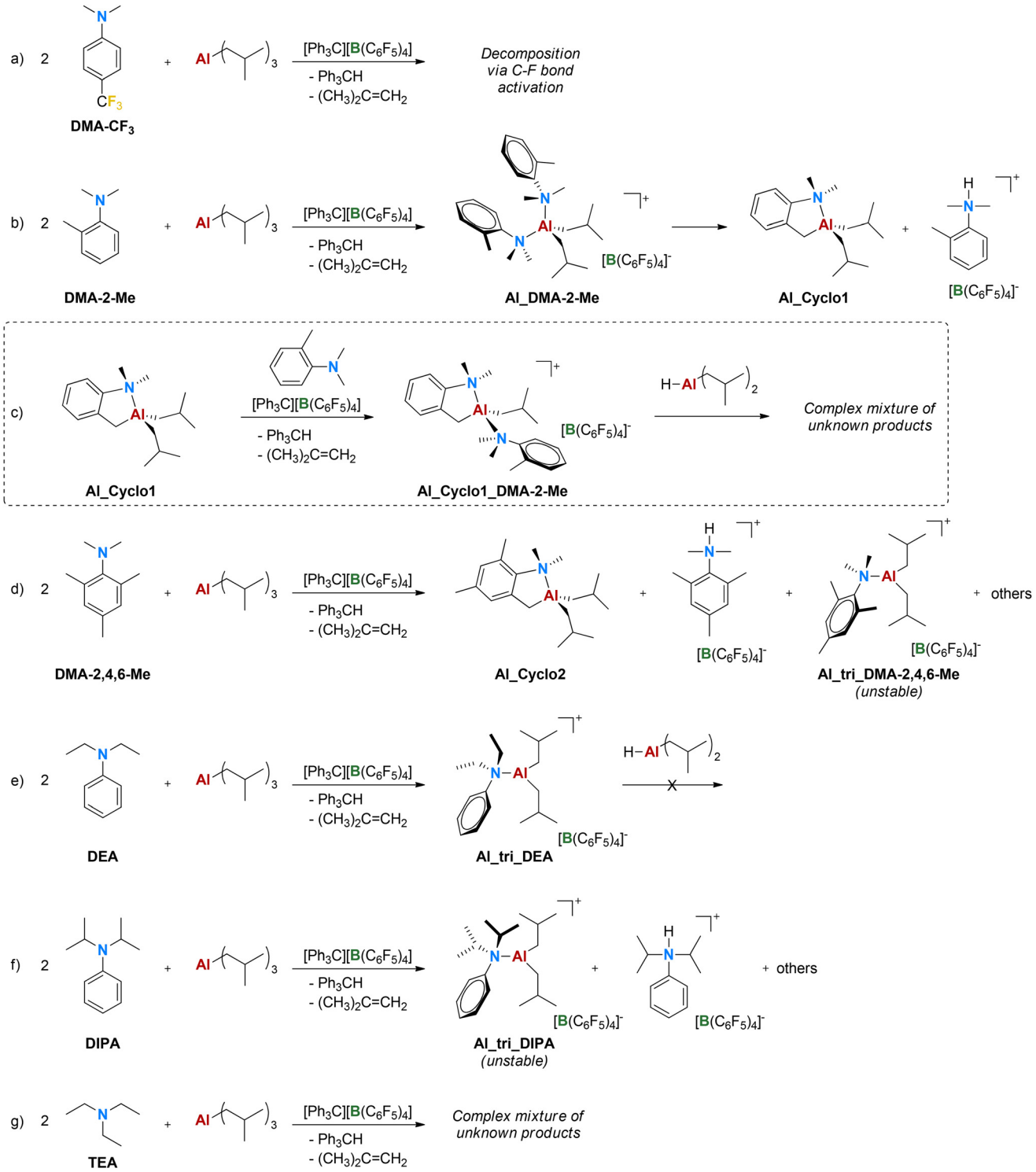

Scheme 2 Side reactions observed with some aniline and amine donors. Exploration of the reactivity of **Al_Cyclo1** is reported in the dashed rectangle. DIBAL-H is shown as a monomer for simplicity.

poses over a few hours to a very complex mixture of species: the protonated **DIPA** borate salt is the most abundant and the only one that could be identified. Similarly, three ethyl groups of **TEA** appear to be too bulky to allow the formation of a stable Al-alkyl cation (Scheme 2g).

N-heterocycles. The synthetic route of Scheme 1b was found to be not feasible for N-heterocycles since these strong Lewis bases compete with TIBAL for the reaction with the Lewis acidic TTB (Scheme 3a). To avoid the synthesis of each protonated N-donor borate salt (Scheme 1a), a simple solution con-

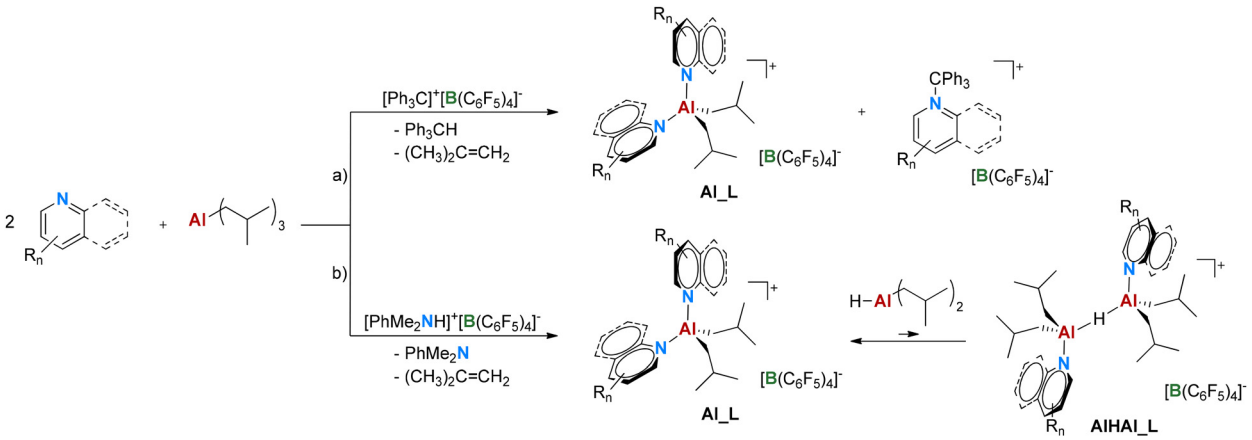

Scheme 3 Synthetic procedures adapted for N-heterocycles. DIBAL-H is shown as a monomer for simplicity. R = Me or F.

sists in replacing TTB with a Brønsted acidic ionizing agent like AB (Scheme 3b), which is less prone to reaction with N-heterocycles. The **DMA** byproduct of these reactions (Scheme 3b) remains "free" because it is unable to compete with N-heterocycles for coordination at Al, and it can be easily removed by washing with pentane. This approach was successfully applied to the synthesis of **Al_L** with nearly all N-heterocycles, including **Al_Py-4-NMe$_2$** that coordinates to aluminum selectively *via* the more electron-rich pyridinic nitrogen atom (Fig. S20 and 21†).

Major decomposition is observed only with **Py-F$_5$**, which undergoes C–F bond activation. Hydrodefluorination of **Py-F$_5$** with Al/Ga reagents catalyzed by Lewis bases has been previously reported;[39,51] interestingly, herein, it is only observed with perfluorinated pyridine and not with **Py-3,5-F**, containing less activated C–F bonds. In the case of **Py-2,6-Me**, formation of small amounts (1–2 mol%) of pyridinium borate byproduct is observed, indicative of proton transfer from AB. The resulting N–H$^+$ bond does not react with TIBAL, likely because it is sterically shielded by the two *o*-Me groups. The pyridinium salt fraction increases upon storing solid **Al_Py-2,6-Me** over several weeks, suggesting that it is a product of its self-decomposition. It is worth mentioning here that all the other **Al_L** species prepared here can be stored under an inert atmosphere for at least 1 year without major signs of decomposition.

The crystal structure could be analyzed for **Al_L** with **L** = **Py-3,5-Me** and **QUI** (Fig. 3d and e). The two species exhibit a similar tetrahedral structure with nearly identical Al–C bond lengths of ~1.96 Å (entries 4 and 5, Table 2). The Al–N bonds of **Al_QUI** (~2.00 Å) are slightly longer than those of **Al_Py-3,5-Me** (~1.97 Å), likely reflecting the lower electron donating ability and higher steric bulk of **QUI**. With respect to the solid state structure of the aniline-based AAB, the main difference emerges in the N–Al–N angle, which is significantly smaller for the N-heterocycles (entries 1 and 2 *vs.* 4 and 5, Table 2), following the trend **Al_Py-3,5-Me** (96.42(8)°) < **Al_QUI** (99.53(11)°) ≪ **Al_DMA-Cl** (104.31(11)°) < **Al_DMA** (106.22(5)°). This is likely due to the flat nature of N-heterocycle donors, having sp^2 hybridized nitrogen, rendering them less sterically demanding than anilines.

Notably, addition of DIBAL-H to **Al_L** with N-heterocycles did not provide detectable amounts of **AlHAl_L**, even when an excess of hydride up to 10 eq. is added (*i.e.* $K_{eq} \ll 1$ for the reaction in eqn (1); entry 8, Table 1; see also the ESI†).[52]

Polymerization experiments

The performance of the twelve successfully synthesized AAB salts was explored in ethylene/1-hexene copolymerization at 60 °C with a representative *ansa*-zirconocene catalyst (**Cat-Zr**, Fig. 4; see the Experimental part for details).[53–57] For the donors allowing isolation of both mono- and dinuclear species (*i.e.* anilines and amines), **AlHAl_L** was tested since **Al_L** cannot function as stand-alone cocatalyst.[32] Conversely, for N-heterocycles and **DEA** that only form mononuclear species, an equimolar mixture of **Al_L** and DIBAL-H was used, since the Al-hydride is an integral part of the cocatalyst.

Based on preliminary experiments with the prototypical **AlHAl_DMA** (Table S7†), a rather low catalyst concentration of 2.5×10^{-7} M and a [B]/[Zr] ratio of 100 were selected as screening conditions for all cocatalysts. Even lower [B]/[Zr] ratios would suffice to obtain comparable productivity (Table S7†) but, to assure comparability also with less efficient **AlHAl_L**

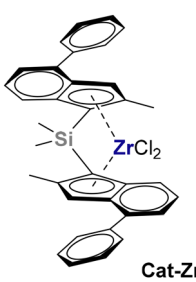

Fig. 4 C_2-Symmetric *ansa*-zirconocene precatalyst used for cocatalyst screening.

Table 3 Summary of ethene/1-hexene copolymerization results[a]

Entry	L	R_p[b]	Relative R_p[c] (%)	M_n[d] (kDa)	PDI[d]
1	**DMA**	462	100	80	2.3
2	**DMA-C$_{16}$**	401	87	75	2.5
3	**DMA-Ph**	367	79	82	2.3
4	**DMA-Cl**	466	101	86	2.5
5	**DEA**	422	91	75	2.4
6	**DMCA**	533	116	75	2.5
7	**DMHA**	267	58	82	2.4
8	**Py-2,6-Me**	3	1	n.a.	n.a.
9	**Py-3,5-Me**	12	3	82	2.3
10	**Py-3,5-F**	224	48	83	2.3
11	**Py-4-NMe2**	∼0	∼0	n.a.	n.a.
12	**QUI**	95	21	77	2.4

[a] Experimental conditions: ethylene/1-hexene copolymerization in toluene (6 mL), T = 60 °C, p_{C2} = 4.5 bar (65 psi), t = 10 min, $[H]_{feed}$ = 1.8 v/v%, $[H]_{incorporated} \approx 7$ mol%, $n_{\mathbf{Cat\text{-}Zr}}$ = 1.5 nmol, $n_{\mathbf{AlHAl}}$ = 150 nmol (*i.e.* [B]/[Zr] = 100). [b] Productivity in $kg_{PE}\ mmol_{Cat}^{-1}\ h^{-1}$. [c] Relative productivity with respect to **AlHAl_DMA**. [d] Determined by GPC (∼20% experimental uncertainty). n.a. = not available. Results are averages of at least triplicate experiments.

variations, we used higher cocatalyst loadings. Results are summarized in Table 3.

The vast majority of AABs yield good productivities in olefin polymerization, showing that **AlHAl_DMA** is not a unique case of a well-defined AAB cocatalyst. Polymer properties in terms of average molecular weight and comonomer incorporation (∼7 mol% for all samples, as determined by ^{13}C NMR spectroscopy) are not affected by the choice of AAB within experimental uncertainty. This suggests that the same active species is obtained in all cases, albeit with varying efficiency.

Fig. 5 shows a comparison of relative productivities for all AAB with respect to the benchmark **AlHAl_DMA**. Within the 15% experimental uncertainty estimated for these tests, all the *para*-substituted *N*,*N*-dimethylanilines based cocatalyst provided similarly active systems. Interestingly, **Al_tri_DEA**/DIBAL-H behaves similar to the other aniline cocatalysts, suggesting that the presence of two aniline ligands around the Al and, more generally, isolation of **AlHAl_L** are not strictly necessary for effective cocatalytic performance.

Concerning amine-based systems, the productivity obtained with **AlHAl_DMCA** is comparable to that with **AlHAl_DMA**, while **AlHAl_DMHA** is appreciably worse. In contrast, the N-heterocycle based AABs produce acceptable activator systems only with the least electron donating donors, *i.e.* **Py-3,5-F** and **QUI**. Increasing the [B]/[Zr] ratio to ∼170 provides similar trends (Fig. S38†).

To put results in perspective, we also tested a representative established cocatalyst, namely AB/TIBAL, under the same reaction conditions (Table S7†). At the same catalyst concentration used for **AlHAl_L**, no detectable activity is observed with the benchmark cocatalyst, signifying the effectiveness of **AlHAl_L** as both an activator and scavenger. Increasing [Zr] with AB/TIBAL by a factor of ∼7 eventually leads to a productivity comparable to that observed with **Py-3,5-F** and **QUI**, indicating that even these AAB salts are moderately good cocatalysts.

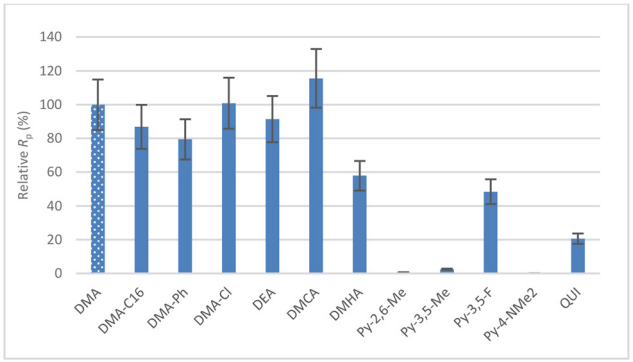

Fig. 5 Relative productivities with respect to that with **AlHAl_DMA** obtained with **Cat-Zr** at B/Zr = 100 in combination with various AAB cocatalysts (see Table 3). 15% experimental uncertainty is assumed on R_p.

Structure–property correlations

By analyzing the results discussed in the previous sections, some considerations can be made regarding structure–property correlations. In terms of stability of **Al-L**, electronic effects appear marginal within each class of N-donors: for instance, no appreciable difference is observed comparing **DMA** with other *para*-substituted anilines, or **Py-3,5-Me** with **Py-3,5-F**. Steric effects are instead more relevant: for instance, going from the *N*-methyl groups of **DMA** to the *N*-ethyl groups of **DEA** destabilizes **Al_L** dramatically (Scheme 2e). The self-decomposition observed with **Py-2,6-Me**, but not with its homologue **Py-3,5-Me**, might also be ascribed to the increased steric hindrance around the N-atom of the former donor.

Regarding the relative stability of **Al_L** and **AlHAl_L** (eqn (1) and Table 1), donors belonging to the same class behave similarly, while a pronounced difference is observed across the different classes: anilines and amines have negative ΔG, while N-heterocycles have strongly positive ΔG. The reason for such marked discontinuity is likely rooted in simultaneous electronic and steric changes going from the former two classes to the latter one. The sp^2 hybridized nitrogen in N-heterocycles has a much smaller steric footprint than sp^3-hybridized anilines and amines (*vide supra*); concomitantly, N-heterocycles are stronger Lewis bases. Therefore, coordination of two N-heterocycles to **Al_L** leads to a less crowded, highly stabilized Al cation compared to anilines and amines.

Comparing the results presented in Tables 1 and 3, it becomes evident that the relative stability of **Al_L** and **AlHAl_L** does not correlate directly with polymerization performance. For instance, all N-heterocycles exhibit a similar preference for formation of **Al_L**, while only **Py-3,5-F** and **QUI** yield efficient catalytic systems in combination with **Cat-Zr**.

Trends in R_p are slightly more varied than those in ΔG for eqn (1). Although the variety of the dataset does not suffice to allow thorough statistical analysis of the quantitative structure–activity relationship (QSAR), we embarked on a computational study to analyze the AAB cocatalysts aiming to identify at least a preliminary model.

Al_L species were considered as they are the ones that could be observed experimentally for all the N-donors tested in polymerization. The hexadecyl chains of **DMA-C$_{16}$** and **DMHA** were modelled with shorter propyl fragments. Given the high flexibility of all these molecules, rotamer/conformer sampling was done with the CREST software suite[58,59] and lowest energy structures were then fully optimized at the M06-2X(PCM)/TZ//TPSSh/DZ level (see the Computational part).

A simple quantitative relationship could be readily identified relying on two established molecular descriptors (Fig. 6 and the ESI†):

(1) The buried volume (V_{Bur}) imparted by the two N-donor fragments, which is a purely steric descriptor;[60]

(2) The Wiberg bond index for the weaker Al–C$_{iBu}$ bond, which is a mixed steric and electronic descriptor reflecting the stabilization imparted by the N-donors.[61,62]

The resulting R^2 of 0.88 is satisfactory, considering that modelling productivity in olefin polymerization is problematic due to the many subtleties in determining intrinsic activity and fraction of active sites.[3,63–66] In the present case, the problem is exacerbated by the fact that N-donors, especially the least sterically hindered and more basic ones, are potential poisons for the strongly electrophilic Zr-active sites.[67,68]

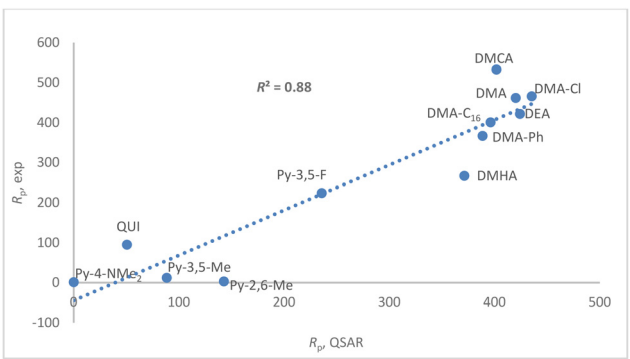

Fig. 6 Plot of experimental *vs.* calculated R_p based on the proposed QSAR model.

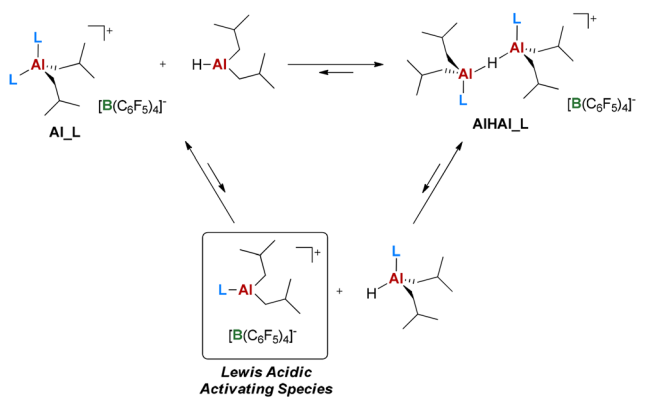

Scheme 4 Proposed mechanism for **Al_L** and **AlHAl_L** manifesting their "latent" Lewis acidity by the release of an unsaturated Al-alkyl cation. DIBAL-H is shown as a monomer for simplicity.

The proposed model suggests that the bulkier the N-donor and the more covalent the Al–C bond (*i.e.* the less the Al-alkyl cation is stabilized by the N-donor; see the ESI†), the higher the productivity. This trend likely reflects the "latent" Lewis acidity of the Al-centers. The activating (*i.e.* ionizing) ability of Al-cocatalysts is generally ascribed to their ability to release unsaturated Al-alkyl cations,[32,69–73] which should correspond to a [AliBu$_2$(**L**)]$^+$ fragment in the present case (Scheme 4).[32] It is reasonable to assume that the ease of formation of this unsaturated fragment increases for less stable AAB salts, explaining the trend in productivity.

Conclusion

This work explored the possibility of modifying the structure and reactivity of the recently revealed **AlHAl_DMA** cocatalyst for olefin polymerization,[32,34,35] focusing on variation of its N-donor ligands. Reasonably stable AAB salts could be obtained with twelve of the 18 donors screened, including molecules with polar –F, –Cl and –NMe$_2$ functionalities. Side reactions were observed with the other six donors, including the most sterically hindering ones and those featuring activated C–F bonds. Dinuclear **AlHAl_L** species are obtained with anilines and amines, while N-heterocycles only form mononuclear **Al_L**. Polymerization experiments revealed that aniline and amine donors lead to cocatalysts with similar performances to the benchmark **AlHAl_DMA**, except for **DMHA** providing lower productivity. Among N-heterocycles, only the two least electron donating donors **Py-3,5-F** and **QUI** provided a detectable, moderate productivity. A simple two-descriptors QSAR model suggests that the observed trends in R_p are related to the ease of formation of unsaturated Al-alkyl cations, capable of precatalyst activation, from the formally coordinatively saturated AAB cocatalysts.

These results demonstrate that it is possible to obtain a variety of effective **AlHAl**-type cocatalysts for olefin polymerization. Despite the relatively limited variability observed, especially among anilines, analysis of degradation routes and a preliminary QSAR model provided important information that might be exploited to design better performing systems. It is worth emphasizing here that Al-alkyl cations are proposed to be essential transient species for the activation of molecular olefin polymerization catalysts:[32,69–73] herein, we show how these highly reactive species can be trapped in donor stabilized forms that preserve their activation capability while being amenable to reactivity tuning. In this respect, even toning down activation abilities of molecular activators can be of interest, for instance to prevent overheating and/or extend the lifetime of superactive catalysts[74] in high temperature industrial processes; systematic exploration of the thermal stability of AAB salts, so far explored preliminarily only for **DMA-C$_{16}$**,[35] will provide further insights in this respect. Milder activators could also be exploited to obtain well-defined species for structural and mechanistic studies. We are currently trying to expand the family of well-defined AAB beyond N-containing

Lewis bases and to explore the scope of these species in polymerization catalysis and in the broader context of aluminum organometallic chemistry.

Experimental part

Materials and methods

All manipulations were performed under rigorous exclusion of oxygen and moisture in flame-dried Schlenk-type glassware interfaced to a high-vacuum line (<10^{-5} Torr), or in a nitrogen-filled MBraun glovebox (<0.5 ppm O_2). Molecular sieves (4 Å, MS) were activated for 24 h at *ca.* 200–230 °C under dynamic vacuum. Benzene-d_6 and toluene-d_8 were freeze–pump–thaw degassed on a high-vacuum line, dried over Na/K alloy, vacuum-transferred to a dry storage-tube with a PTFE valve and stored over activated MS in the glovebox. Chlorobenzene-d_5 was freeze–pump–thaw degassed on the high-vacuum line, dried over CaH_2, vacuum-transferred to a dry storage-tube with a PTFE valve and stored over activated MS, protected from light, in the glovebox. TTB and AB were obtained from Boulder Scientific Company and used as received. **DMA**, **DMA-2-Me**, **DMA-2,4,6-Me**, **DEA**, **DIPA**, **DMCA**, **DMHA**, **TEA**, **Py-2,6-Me**, **Py-3,5-Me**, **Py-3,5-F**, **Py-4-NMe$_2$**, **QUI**, 4-aminobiphenyl, potassium carbonate, methyliodide, DIBAL-H, TIBAL, DIBAL-Cl, and BuLi (1.6 M in hexane) were purchased from Merck; **DMA-Cl** and **DMA-CF$_3$** were purchased from ABCR; **Py-F$_5$** was purchased from TCI Europe. **AlHAl_DMA**,[32] **AlHAl_DMA-C$_{16}$**[35] and [**DMHA**-H]$^+$[B(C_6F_5)$_4$]$^-$[36] were synthesized as reported in the literature. **Cat-Zr** was kindly donated by SABIC. Ethene (Linde, 99.95%) and propene (Rivoira, 99.6%) were purified by flowing them through a column containing activated 4 Å molecular sieves and an activated Cu catalyst (BASF R0-11G). 1-Hexene (Sigma-Aldrich, 99%) was purified by passing it through a mixed-bed column of activated Cu catalyst and 4 Å molecular sieves. Toluene (Romil) was dried using an MBraun SPS-5 solvent purification unit. 1,2-Dichlorobenzene (Romil, >99.8% isomeric purity) was used as received for GPC analysis or purified by passing it through a mixed-bed column of activated Cu catalyst and 4 Å molecular sieves for synthesis purposes.

Synthetic procedures

The synthetic procedures were adapted from those previously reported for **Al_DMA** and **AlHAL_DMA**,[32,35] by replacing **DMA** with the other N-donors. The representative synthetic procedures for **Al_DMA** and **AlHAL_DMA** are reported below, while details of their characterization are reported in the ESI.† The details on the synthesis and characterization of other relevant species (**DMA-Ph**,[75] **Al_Cyclo1**, **Al_Cyclo1_DMA-2-Me**, **Al_tri_TEA**) are reported in the ESI,† as well.

Al_L with L = aniline or amine. *Representative general procedure*: Solid TTB (150 mg, 0.16 mmol) was added in small aliquots to a preformed and stirred solution of TIBAL (45 μL, 0.18 mmol) and **L** donor (0.36 mmol) in toluene (1.5 mL). The resulting mixture was vigorously stirred for 16 h at room temperature. Upon stopping the stirring, a colorless oil precipitated. Pentane (6 mL) was added to facilitate the precipitation of ionic products. The supernatant was then removed, and the oil further washed with pentane (2 × 6 mL). After the last washing, the residue was dried under vacuum to obtain **Al_L** as a white solid (yield: 91% for **DMA**; 80% for **DMA-C$_{16}$**; 93% for **DMA-Ph**; 91 for **DMA-Cl**; 87% for **DMCA**; 87% for **DMHA**). For **Al_DMA-Cl**, dissolving the solid in *ortho*-difluorobenzene and reprecipitating with pentane might be necessary for effective purification. This is because this species is poorly soluble in toluene and therefore precipitates rapidly as a solid in the reaction medium, trapping byproducts and/or excess reagents in the solid fraction. See the ESI for characterization details.†

AlHAl_L with L = aniline or amine. *Representative general procedure*: **Al_L** (0.14 mmol) was suspended in toluene (1 mL) or dissolved in *ortho*-difluorobenzene (for **Al_DMA-Cl**), and DIBAL-H (25 μL, 0.14 mmol) was added. After stirring the resulting mixture for 15 min, pentane (6 mL) was added to facilitate the precipitation of ionic products. The supernatant was then removed, and the oil further washed with pentane (2 × 6 mL). After the last washing, the residue was dried under vacuum to obtain **AlHAl_L** as a highly viscous, colorless oil (>90% isolated yield in all cases; *cf.* Table 1). See the ESI for characterization details.†

Al_L with L = N-heterocycles. *Representative general procedure*: Solid AB (130 mg, 0.16 mmol) was added in small aliquots to a preformed and stirred solution of TIBAL (45 μL, 0.18 mmol) and **L** donor (0.36 mmol) in toluene (1.5 mL). The resulting mixture was vigorously stirred for 16 h at room temperature. Upon stopping the stirring, a colorless oil precipitated. Pentane (6 mL) was added to facilitate the precipitation of ionic products. The supernatant was then removed, and the oil further washed with pentane (2 × 6 mL). After the last washing, the residue was dried under vacuum to obtain **Al_L** as a white solid (yield: 93% for **Py-2,6-Me**; 95% for **Py-3,5-Me** and **Py-3,5-F**; 94% for **Py-4-NMe$_2$**; 97% for **QUI**). See the ESI for characterization details.†

NMR spectroscopy experiments

NMR experiments were performed using a Bruker Avance III HD 400 instrument equipped with a smart probe (400 MHz for ^{1}H). ^{1}H NMR spectra were referenced to the residual protons of the deuterated solvent used; ^{13}C NMR spectra were referenced internally to the D-coupled ^{13}C resonances of the NMR solvent. To describe the multiplicity of the signals, the following abbreviations are used: s, singlet; bs, broad singlet; d, doublet; bd, broad doublet; dd, doublet of doublets; t, triplet; m, multiplet.

X-ray diffraction experiments

The X-ray diffraction patterns of crystals were recorded using a Bruker D8 Venture diffractometer equipped with an Incoatec ImuS3.0 microfocus sealed-tube MoKα (λ = 0.71073 Å) source and a CCD Photon II detector. The analysis were carried out at a low temperature (120–150 K range) using an Oxford Cryosystems Cryostream 800 cooler. The data collected

through generic φ and ω scans were integrated and reduced using the Bruker AXS V8 Saint Software. The structures were solved and all the thermal parameters were anisotropically refined using the SHELXT and SHELXL packages of the Bruker APEX3 software.

Polymerization experiments

Ethene/1-hexene polymerization experiments were performed in a Freeslate parallel pressure reactor setup with 48 reaction cells (PPR48), fully contained in a triple MBraun glovebox operating under nitrogen. The cells, each with a liquid working volume of 6.0 mL, featured an 800 rpm magnetically coupled stirring, and individual online reading/control of temperature, pressure, monomer uptake, and monomer uptake rate. Experiments were carried out according to established experimental protocols,[53–56] under the following experimental conditions: toluene solvent; T_p = 60 °C; p_{ethene} = 65 psi (monomer fed on demand); 1-hexene 1.8 v/v%; **AlHAl_L** activator (n_{AlHAl} = 150 or 250 nmol); **Cat-Zr** precatalyst (n_{CatZr} = 1.5 nmol); t = 10 min. It is worth mentioning that although **AlHAl_L** are stable in the form of isolated oils over weeks under an inert atmosphere, freshly assembling them by reaction between equimolar amounts of **Al_L** and DIBAL-H may be convenient for polymerization experiments: **Al_L** are solids that can be stored under nitrogen for at least 1 year without noticeable decomposition (unless otherwise stated) and react with DIBAL-H instantaneously. Conversion of 1-hexene was kept below 15% to ensure a constant comonomer concentration. All experiments were performed at least in duplicate. Polymer samples were characterized by gel permeation chromatography (GPC) to determine average molecular weights and molecular weight distributions, and by ^{13}C NMR spectroscopy to determine comonomer incorporation. A detailed experimental procedure is reported in the the ESI.†

Computational details

The chemical space of possible conformers was preliminarily explored using the CREST program.[58,59] The (at least) three lowest energy conformers derived from CREST analysis for each molecule were then fully optimized with the Gaussian 16 software package,[76] following the protocol described in ref. 77 and 78. All relevant structures were fully optimized in the gas phase at the TPSSh[79] level of theory employing correlation-consistent polarized valence double-ζ Dunning(DZ) basis sets (cc-pVDZ quality)[80,81] from the EMSL basis set exchange library.[82] All calculations were performed using standard Gaussian 16 SCF convergence criteria. Final single-point energies were calculated at the M06-2X level of theory[83] employing triple-ζ Dunning (TZ) basis sets (cc-pVTZ quality).[84] Solvent corrections were included at this stage by the polarized continuum model (PCM; solvent = toluene).[85] The density fitting approximation (resolution of identity, RI) was used at the optimization stage, as well as for final energy calculations.[84,86–88] Enthalpies and Gibbs free energies were then obtained from TZ single-point energies and thermal corrections from the TPSSh/DZ vibrational analyses; entropy corrections were scaled by a factor of 0.67 to account for decreased entropy in the condensed phase.[89,90] Steric and electronic descriptors were then collected from the lowest energy conformer. IBO iboview[61,62] was utilized to extract relevant electronic molecular descriptors from MN15L/SVP calculations employing the IBOviews internal scf routine. SambVca 2.1[60] was used to determine V_{bur} and produce topographic steric maps. The default sphere size was chosen (3.5 Å). The aluminum atom was chosen as the center of the sphere, the z-axis was defined using the center between the two Al–C bonds, and the plane was defined using one of the two Al–C atoms.

Data availability

The data supporting this article have been included as part of the ESI. CCDC 2372888–2372892 contain the supplementary crystallographic data for this paper.†

Conflicts of interest

There are no conflicts to declare.

Acknowledgements

This research forms part of the research program of DPI (project 857). Part of this work has been funded by the European Union – NextGenerationEU under the Italian Ministry of University and Research (MUR) National Innovation Ecosystem grant ECS00000041 – VITALITY. We acknowledge Università degli Studi di Perugia and MUR for support within the project Vitality. A. M. and C. Z. thank the "FASTTO0" project (CUP J93C22000330006), funded through the Italian Ministry of Environment and Energy Security. The authors thank Dr Martina Landrini for support with crystallographic determinations. F. Z. thanks the Federico II University of Naples and PON – Ricerca e Innovazione (DM 1062) for a research fellowship.

References

1 M. Stürzel, S. Mihan and R. Mülhaupt, From Multisite Polymerization Catalysis to Sustainable Materials and All-Polyolefin Composites, *Chem. Rev.*, 2016, **116**, 1398–1433.
2 W. Kaminsky, The discovery of metallocene catalysts and their present state of the art, *J. Polym. Sci., Part A: Polym. Chem.*, 2004, **42**, 3911–3921.
3 F. Zaccaria, L. Sian, C. Zuccaccia and A. Macchioni, Ion pairing in transition metal catalyzed olefin polymerization, in *Advasnces in Organometallic Chemistry*, ed. P. J. Perez, Elsevier, Amsterdam, The Netherlands, 2020, vol. 73, pp. 1–78.
4 J. Klosin, P. P. Fontaine and R. Figueroa, Development of group IV molecular catalysts for high temperature ethylene-

α-olefin copolymerization reactions, *Acc. Chem. Res.*, 2015, **48**, 2004–2016.
5 M. C. Baier, M. A. Zuideveld and S. Mecking, Post-metallocenes in the industrial production of polyolefins, *Angew. Chem., Int. Ed.*, 2014, **53**, 9722–9744.
6 A. Andresen, H.-G. Cordes, J. Herwig, W. Kaminsky, A. Merck, R. Mottweiler, J. Pein, H. Sinn and H.-J. Vollmer, Halogen–Free Soluble Ziegler Catalysts for the Polymerization of Ethylene. Control of Molecular Weight by Choice of Temperature, *Angew. Chem., Int. Ed. Engl.*, 1976, **15**, 630–632.
7 H. S. Zijlstra and S. Harder, Methylalumoxane - History, production, properties, and applications, *Eur. J. Inorg. Chem.*, 2015, **2015**, 19–43.
8 E. Y. X. Chen and T. J. Marks, Cocatalysts for metal-catalyzed olefin polymerization: Activators, activation processes, and structure-activity relationships, *Chem. Rev.*, 2000, **100**, 1391–1434.
9 M. Bochmann, The chemistry of catalyst activation: The case of group 4 polymerization catalysts, *Organometallics*, 2010, **29**, 4711–4740.
10 Y. Gao, M. D. Christianson, Y. Wang, M. P. Coons, J. Chen, J. Zhang, S. Marshall, T. L. Lohr, J. Klosin and T. J. Marks, Alkane-Soluble Bis[tris(alkylphenyl)carbenium] Diborate Cocatalyst for Olefin Polymerizations, *ACS Catal.*, 2022, **12**, 7589–7597.
11 Y. Gao, J. Chen, Y. Wang, D. B. Pickens, A. Motta, Q. J. Wang, Y. W. Chung, T. L. Lohr and T. J. Marks, Highly branched polyethylene oligomers via group IV-catalysed polymerization in very nonpolar media, *Nat. Catal.*, 2019, **2**, 236–242.
12 S. Kitphaitun, T. Fujimoto, Y. Ochi and K. Nomura, Effect of Borate Cocatalysts toward Activity and Comonomer Incorporation in Ethylene Copolymerization by Half-Titanocene Catalysts in Methylcyclohexane, *ACS Org. Inorg. Au*, 2022, **2**, 386–391.
13 S. O. Gunther, Q. Lai, T. Senecal, R. Huacuja, S. Bremer, D. M. Pearson, J. C. DeMott, N. Bhuvanesh, O. V. Ozerov and J. Klosin, Highly Efficient Carborane-Based Activators for Molecular Olefin Polymerization Catalysts, *ACS Catal.*, 2021, **11**, 3335–3342.
14 S. J. Lancaster, A. Rodriguez, A. Lara-Sanchez, M. D. Hannant, D. A. Walker, D. H. Hughes and M. Bochmann, $[H_2N\{B(C_6F_5)_3\}_2]^-$: A new, remarkably stable diborate anion for metallocene polymerization catalysts, *Organometallics*, 2002, **21**, 451–453.
15 R. Tanaka, Precise control of coordination polymerization via the modification of methylaluminoxane, *Polym. J.*, 2020, **52**, 661–670.
16 W. E. Piers, The Chemistry of Perfluoroaryl Boranes, in *Advances in Organometallic Chemistry*, Academic Press, 2004, vol. 52, pp. 1–76.
17 D. Langford, I. Göttker-Schnetmann, F. P. Wimmer, L. A. Casper, P. Kenyon, R. F. Winter and S. Mecking, Tetrakis[3,5-bis(pentafluorosulfanyl)phenyl]borate: A Weakly Coordinating Anion Probed in Polymerization Catalysis, *Organometallics*, 2019, **38**, 2710–2713.
18 V. C. Williams, W. E. Piers, W. Clegg, M. R. J. Elsegood, S. Collins and T. B. Mardell, New bifunctional perfluoroaryl boranes. Synthesis and reactivity of the ortho-phenylene-bridged diboranes 1,2-$[B(C_6F_5)_2]_2C_6X_4$ (X = H, F), *J. Am. Chem. Soc.*, 1999, **121**, 3244–3245.
19 Y. X. Chen, C. L. Stern and T. J. Marks, Very large counteranion modulation of cationic metallocene polymerization activity and stereoregulation by a sterically congested (perfluoroaryl) fluoroaluminate, *J. Am. Chem. Soc.*, 1997, **119**, 2582–2583.
20 H. S. Zijlstra, A. Joshi, M. Linnolahti, S. Collins and J. S. McIndoe, Modifying methylalumoxane via alkyl exchange, *Dalton Trans.*, 2018, **47**, 17291–17298.
21 R. Kleinschmidt, Y. Van Der Leek, M. Reffke and G. Fink, Kinetics and mechanistic insight into propylene polymerization with different metallocenes and various aluminium alkyls as cocatalysts, *J. Mol. Catal. A: Chem.*, 1999, **148**, 29–41.
22 M. Galimberti, M. Destro, O. Fusco, F. Piemontesi and I. Camurati, Ethene/propene copolymerization from metallocene-based catalytic systems: Role of the alumoxane, *Macromolecules*, 1999, **32**, 258–263.
23 V. Busico, R. Cipullo, F. Cutillo, N. Friederichs, S. Ronca and B. Wangt, Improving the performance of methylalumoxane: A facile and efficient method to trap 'free' trimethylaluminum, *J. Am. Chem. Soc.*, 2003, **125**, 12402–12403.
24 F. Zaccaria, C. Zuccaccia, R. Cipullo and A. Macchioni, Extraction of Reliable Molecular Information from Diffusion NMR Spectroscopy: Hydrodynamic Volume or Molecular Mass?, *Chem. – Eur. J.*, 2019, **25**, 9930–9937.
25 F. Zaccaria, C. Zuccaccia, R. Cipullo, P. H. M. Budzelaar, A. Macchioni, V. Busico and C. Ehm, On the Nature of the Lewis Acidic Sites in "TMA-Free" Phenol-Modified Methylaluminoxane, *Eur. J. Inorg. Chem.*, 2020, **2020**, 1088–1095.
26 L. Luo, S. A. Sangokoya, W. Xiao, S. P. Diefenbach and B. Kneale, Aluminoxane catalyst activators derived from dialkylaluminum cation precursor agents, processes for making same, and use thereof in catalysts and polymerization of olefins, 2009, *Patent Appl*, US8575284.
27 L. Oliva, P. Oliva, N. Galdi, C. Pellecchia, L. Sian, A. Macchioni and C. Zuccaccia, Solution Structure and Reactivity with Metallocenes of $AlMe_2F$: Mimicking Cation–Anion Interactions in Metallocenium–Methylalumoxane Inner-Sphere Ion Pairs, *Angew. Chem., Int. Ed.*, 2017, **56**, 14227–14231.
28 J. C. W. Chien and D. He, Olefin copolymerization with metallocene catalysts. II. Kinetics, cocatalyst, and additives, *J. Polym. Sci., Part A: Polym. Chem.*, 1991, **29**, 1595–1601.
29 G. Zanchin, A. Piovano, A. Amodio, F. De Stefano, R. Di Girolamo, E. Groppo and G. Leone, NEt_3-Triggered Synthesis of UHMWPE Using Chromium Complexes Bearing Non-innocent Iminopyridine Ligands, *Macromolecules*, 2021, **54**, 1243–1253.
30 P. G. Belelli, M. L. Ferreira and D. E. Damiani, Addition of Lewis bases and acids. Effect on α-olefins polymerization with soluble metallocenes, 1 Ethylene, *Macromol. Chem. Phys.*, 2000, **201**, 1458–1465.

31 L. Luo, J. M. Younker and A. V. Zabula, Structure of methylaluminoxane (MAO): Extractable $[Al(CH_3)_2]^+$ for precatalyst activation, *Science*, 2024, **384**, 1424–1428.
32 F. Zaccaria, C. Zuccaccia, R. Cipullo, P. H. M. Budzelaar, A. Vittoria, A. Macchioni, V. Busico and C. Ehm, Methylaluminoxane's Molecular Cousin: A Well-defined and "Complete" Al-Activator for Molecular Olefin Polymerization Catalysts, *ACS Catal.*, 2021, **11**, 4464–4475.
33 C. J. Harlan, A. R. Barron and S. G. Bott, Three-Coordinate Aluminum Is Not a Prerequisite for Catalytic Activity in the Zirconocene—Alumoxane Polymerization of Ethylene, *J. Am. Chem. Soc.*, 1995, **117**, 6465–6474.
34 G. Urciuoli, F. Zaccaria, C. Zuccaccia, R. Cipullo, P. H. M. Budzelaar, A. Vittoria, C. Ehm, A. Macchioni and V. Busico, Cocatalyst effects in Hf-catalysed olefin polymerization: taking well-defined Al-alkyl borate salts into account, *Dalton Trans.*, 2024, **53**, 2286–2293.
35 G. Urciuoli, F. Zaccaria, C. Zuccaccia, R. Cipullo, P. H. M. Budzelaar, A. Vittoria, C. Ehm, A. Macchioni and V. Busico, A Hydrocarbon Soluble, Molecular and "Complete" Al-Cocatalyst for High Temperature Olefin Polymerization, *Polymers*, 2023, **15**, 1378.
36 H.-J. Lee, J.-W. Baek, Y.-H. Seo, H.-C. Lee, S.-M. Jeong, J. Lee, C.-G. Lee and B.-Y. Lee, Preparation of High-Purity Ammonium Tetrakis(pentafluorophenyl)borate for the Activation of Olefin Polymerization Catalysts, *Molecules*, 2021, **26**, 2827.
37 O. Wrobel, F. Schaper and H. H. Brintzinger, Bulky Siloxyaluminum Alkyls as Models for Al_2Me_6-Treated Silica Gel Surfaces. Characterization of a Dimethylaniline-Stabilized Dimethylaluminum Cation, *Organometallics*, 2004, **23**, 900–905.
38 M. Klahn, C. Fischer, A. Spannenberg, U. Rosenthal and I. Krossing, Hydrodefluorination of non-activated C-F bonds by diisobutyl-aluminiumhydride via the aluminium cation $[i\text{-}Bu_2Al]^+$, *Tetrahedron Lett.*, 2007, **48**, 8900–8903.
39 A. D. Jaeger, C. Ehm and D. Lentz, Organocatalytic C–F Bond Activation with Alanes, *Chem. – Eur. J.*, 2018, **24**, 6769–6777.
40 H. T. Al-Masri, Oxidation reactions, coordination chemistry and antibacterial activities with ligand 2-{(diphenylphosphino) methyl}-N,N-dimethylaniline, *J. Organomet. Chem.*, 2020, **905**, 121021.
41 J. T. B. H. Jastrzebski, G. Van Koten, M. F. Lappert, P. C. Blake and D. R. Hankey, Cyclometallated Organolithium Compounds, in *Inorganic Syntheses*, 1989, pp. 150–155.
42 K. Murali, L. A. Machado, R. L. Carvalho, L. F. Pedrosa, R. Mukherjee, E. N. Da Silva Júnior and D. Maiti, Decoding Directing Groups and Their Pivotal Role in C–H Activation, *Chem. – Eur. J.*, 2021, **27**, 12453–12508.
43 R. A. Stapleton, A. Al-Humydi, J. Chai, B. R. Galan and S. Collins, Sterically hindered aluminum alky is: Weakly interacting scavenging agents of use in olefin polymerization, *Organometallics*, 2006, **25**, 5083–5092.
44 T. A. Engesser, M. R. Lichtenthaler, M. Schleep and I. Krossing, Reactive p-block cations stabilized by weakly coordinating anions, *Chem. Soc. Rev.*, 2016, **45**, 789–899.
45 S. Dagorne, S. Bellemin-Laponnaz and R. Welter, Synthesis and Structure of Neutral and Cationic Aluminum Complexes Incorporating Bis(oxazolinato) Ligands, *Organometallics*, 2004, **23**, 3053–3061.
46 K. Jakobsson, T. Chu and G. I. Nikonov, Hydrosilylation of Olefins Catalyzed by Well-Defined Cationic Aluminum Complexes: Lewis Acid versus Insertion Mechanisms, *ACS Catal.*, 2016, **6**, 7350–7356.
47 A. Friedrich, J. Eyselein, H. Elsen, J. Langer, J. Pahl, M. Wiesinger and S. Harder, Cationic Aluminium Complexes as Catalysts for Imine Hydrogenation, *Chem. – Eur. J.*, 2021, **27**, 7756–7763.
48 C.-P. Hsu, C.-A. Liu, C.-C. Wen, Y.-H. Liu, Y.-F. Lin and C.-W. Chiu, Chiral Bis(oxazoline) Ligand-Supported Alkyl Aluminum Cations, *ChemCatChem*, 2022, **14**, e202101715.
49 L. Werner, J. Hagn, J. Walpuski and U. Radius, Aluminum (III) Cations $[(NHC)\cdot AlMes_2]^+$: Synthesis, Characterization, and Application in FLP-Chemistry, *Angew. Chem., Int. Ed.*, 2023, **62**, e202312111.
50 S. Ju, C. Zhang, B. Tang, L. L. Liu, D. W. Stephan and Y. Wu, The Lewis superacidic aluminium cation: $[(NHC)Al(C_6F_5)_2]^+$, *Chem. Commun.*, 2023, **60**, 698–701.
51 A. D. Jaeger, R. Walter, C. Ehm and D. Lentz, Gallium Hydrides and O/N-Donors as Tunable Systems in C–F Bond Activation, *Chem. – Asian J.*, 2018, **13**, 2908–2915.
52 Addition of DIBAL-H to **Al_Py-2,6-Me** does not form **AlHAl_Py-2,6-Me** but quantitatively scavenges the pyridinium borate salt, giving H_2 as byproduct.
53 V. Busico, R. Pellecchia, F. Cutillo and R. Cipullo, High-throughput screening in olefinpolymerization catalysis: from serendipitous discovery towards rational understanding, *Macromol. Rapid Commun.*, 2009, **30**, 1697–1708.
54 A. Vittoria, V. Busico, F. D. Cannavacciuolo and R. Cipullo, Molecular Kinetic Study of 'chain Shuttling' Olefin Copolymerization, *ACS Catal.*, 2018, **8**, 5051–5061.
55 C. Ehm, A. Vittoria, G. P. Goryunov, V. V. Izmer, D. S. Kononovich, O. V. Samsonov, P. H. M. Budzelaar, A. Z. Voskoboynikov, V. Busico, D. V. Uborsky and R. Cipullo, On the limits of tuning comonomer affinity of 'Spaleck-type' ansa-zirconocenes in ethene/1-hexene copolymerization: a high-throughput experimentation/QSAR approach, *Dalton Trans.*, 2020, **49**, 10162–10172.
56 D. V. Uborsky, D. Y. Mladentsev, B. A. Guzeev, I. S. Borisov, A. Vittoria, C. Ehm, R. Cipullo, C. Hendriksen, N. Friederichs, V. Busico and A. Z. Voskoboynikov, C_1-Symmetric Si-bridged (2-indenyl)(1-indenyl) *ansa*-metallocenes as efficient ethene/1-hexene copolymerization catalysts, *Dalton Trans.*, 2020, **49**, 3015–3025.
57 F. D. Cannavacciuolo, R. Yadav, A. Esper, A. Vittoria, G. Antinucci, F. Zaccaria, R. Cipullo, P. H. M. Budzelaar, V. Busico, G. P. Goryunov, D. V. Uborsky, A. Z. Voskoboynikov, K. Searles, C. Ehm and A. S. Veige, A High-Throughput Approach to Repurposing Olefin Polymerization Catalysts for Polymer Upcycling, *Angew. Chem., Int. Ed.*, 2022, **61**, e202202258.

58 P. Pracht, S. Grimme, C. Bannwarth, F. Bohle, S. Ehlert, G. Feldmann, J. Gorges, M. Müller, T. Neudecker, C. Plett, S. Spicher, P. Steinbach, P. A. Wesołowski and F. Zeller, CREST—A program for the exploration of low-energy molecular chemical space, *J. Chem. Phys.*, 2024, **160**, 114110.

59 P. Pracht, F. Bohle and S. Grimme, Automated exploration of the low-energy chemical space with fast quantum chemical methods, *Phys. Chem. Chem. Phys.*, 2020, **22**, 7169–7192.

60 L. Falivene, Z. Cao, A. Petta, L. Serra, A. Poater, R. Oliva, V. Scarano and L. Cavallo, Towards the online computer-aided design of catalytic pockets, *Nat. Chem.*, 2019, **11**, 872–879.

61 G. Knizia and J. E. M. N. Klein, Electron Flow in Reaction Mechanisms—Revealed from First Principles, *Angew. Chem., Int. Ed.*, 2015, **54**, 5518–5522.

62 G. Knizia, Intrinsic Atomic Orbitals: An Unbiased Bridge between Quantum Theory and Chemical Concepts, *J. Chem. Theory Comput.*, 2013, **9**, 4834–4843.

63 X. Desert, J. F. Carpentier and E. Kirillov, Quantification of active sites in single-site group 4 metal olefin polymerization catalysis, *Coord. Chem. Rev.*, 2019, **386**, 50–68.

64 F. Zaccaria, C. Ehm, P. H. M. Budzelaar, V. Busico and R. Cipullo, Catalyst Mileage in Olefin Polymerization: The Peculiar Role of Toluene, *Organometallics*, 2018, **37**, 2872–2879.

65 C. H. Chen, W. C. Shih and C. Hilty, In situ determination of tacticity, deactivation, and kinetics in [rac-(C_2H_4(1-Indenyl)$_2$)ZrMe][$B(C_6F_5)_4$] and [Cp_2ZrMe][$B(C_6F_5)_4$]-Catalyzed Polymerization of 1-Hexene Using ^{13}C hyperpolarized NMR, *J. Am. Chem. Soc.*, 2015, **137**, 6965–6971.

66 R. Cipullo, P. Melone, Y. Yu, D. Iannone and V. Busico, Olefin polymerisation catalysts: When perfection is not enough, *Dalton Trans.*, 2015, **44**, 12304–12311.

67 E. Novarino, I. Guerrero Rios, S. Van Der Veer, A. Meetsma, B. Hessen and M. W. Bouwkamp, Catalyst deactivation reactions: The role of tertiary amines revisited, *Organometallics*, 2011, **30**, 92–99.

68 F. Schaper, A. Geyer and H. H. Brintzinger, Displacement of $H_3CB(C_6F_5)_3^-$ anions from zirconocene methyl cations by neutral ligand molecules: Equilibria, kinetics, and mechanisms, *Organometallics*, 2002, **21**, 473–483.

69 F. Ghiotto, C. Pateraki, J. Tanskanen, J. R. Severn, N. Luehmann, A. Kusmin, J. Stellbrink, M. Linnolahti and M. Bochmann, Probing the structure of methylalumoxane (MAO) by a combined chemical, spectroscopic, neutron scattering, and computational approach, *Organometallics*, 2013, **32**, 3354–3362.

70 S. Collins, M. Linnolahti, M. G. Zamora, H. S. Zijlstra, M. T. Rodríguez Hernández and O. Perez-Camacho, Activation of Cp_2ZrX_2 (X = Me, Cl) by Methylaluminoxane As Studied by Electrospray Ionization Mass Spectrometry: Relationship to Polymerization Catalysis, *Macromolecules*, 2017, **50**, 8871–8884.

71 F. Zaccaria, P. H. M. Budzelaar, R. Cipullo, C. Zuccaccia, A. Macchioni, V. Busico and C. Ehm, Reactivity Trends of Lewis Acidic Sites in Methylaluminoxane and Some of Its Modifications, *Inorg. Chem.*, 2020, **59**, 5751–5759.

72 C. Götz, A. Rau and G. Luft, Ternary metallocene catalyst systems based on metallocene dichlorides and $AlBu_3i$/[$PhNMe_2H$] [$B(C_6F_5)_4$] NMR investigations of the influence of Al/Zr ratios on alkylation and on formation of the precursor of the active metallocene species, *J. Mol. Catal. A: Chem.*, 2002, **184**, 95–110.

73 M. Bochmann and M. J. Sarsfield, Reaction of AlR_3 with [CPh_3][$B(C_6F_5)_4$]: Facile degradation of $[B(C_6F_5)_4]^-$ by transient '$[AlR_2]^+$', *Organometallics*, 1998, **17**, 5908–5912.

74 C. Ehm, A. Mingione, A. Vittoria, F. Zaccaria, R. Cipullo and V. Busico, High-Throughput Experimentation in Olefin Polymerization Catalysis: Facing the Challenges of Miniaturization, *Ind. Eng. Chem. Res.*, 2020, **59**, 13940–13947.

75 K. Kinashi, K.-P. Lee, S. Matsumoto, K. Ishida and Y. Ueda, Alkyl substituent effects on J- or H-aggregate formation of bisazomethine dyes, *Dyes Pigm.*, 2012, **92**, 783–788.

76 M. J. Frisch, *et al.*, *Gaussian 16, rev C*, Gaussian Inc., Wallingford CT, 2016.

77 C. Ehm, G. Antinucci, P. H. M. Budzelaar and V. Busico, Catalyst activation and the dimerization energy of alkylaluminium compounds, *J. Organomet. Chem.*, 2014, **772**, 161–171.

78 C. Ehm, P. H. M. Budzelaar and V. Busico, Calculating accurate barriers for olefin insertion and related reactions, *J. Organomet. Chem.*, 2015, **775**, 39–49.

79 J. Tao, J. P. Perdew, V. N. Staroverov and G. E. Scuseria, Climbing the density functional ladder: Nonempirical meta–generalized gradient approximation designed for molecules and solids, *Phys. Rev. Lett.*, 2003, **91**, 146401.

80 N. B. Balabanov and K. A. Peterson, Systematically convergent basis sets for transition metals. I. All-electron correlation consistent basis sets for the 3d elements Sc-Zn, *J. Chem. Phys.*, 2005, **123**, 64107.

81 N. B. Balabanov and K. A. Peterson, Basis set limit electronic excitation energies, ionization potentials, and electron affinities for the 3d transition metal atoms: Coupled cluster and multireference methods, *J. Chem. Phys.*, 2006, **125**, 74110.

82 K. L. Schuchardt, B. T. Didier, T. Elsethagen, L. Sun, V. Gurumoorthi, J. Chase, J. Li and T. L. Windus, Basis set exchange: A community database for computational sciences, *J. Chem. Inf. Model.*, 2007, **47**, 1045–1052.

83 Y. Zhao and D. G. Truhlar, The M06 suite of density functionals for main group thermochemistry, thermochemical kinetics, noncovalent interactions, excited states, and transition elements: Two new functionals and systematic testing of four M06-class functionals and 12 other function, *Theor. Chem. Acc.*, 2008, **120**, 215–241.

84 J. L. Whitten, Coulombic potential energy integrals and approximations, *J. Chem. Phys.*, 1973, **58**, 4496–4501.

85 J. Tomasi, Thirty years of continuum solvation chemistry: A review, and prospects for the near future, *Theor. Chem. Acc.*, 2004, **112**, 184–203.

86 E. J. Baerends, D. E. Ellis and P. Ros, Self-consistent molecular Hartree-Fock-Slater calculations I. The computational procedure, *Chem. Phys.*, 1973, **2**, 41–51.

87 M. Feyereisen, G. Fitzgerald and A. Komornicki, Use of approximate integrals in ab initio theory. An application in MP2 energy calculations, *Chem. Phys. Lett.*, 1993, **208**, 359–363.

88 O. Vahtras, J. Almlöf and M. W. Feyereisen, Integral approximations for LCAO-SCF calculations, *Chem. Phys. Lett.*, 1993, **213**, 514–518.

89 S. Tobisch and T. Ziegler, Catalytic oligomerization of ethylene to higher linear α-olefins promoted by the cationic group 4, $[(\eta^5\text{-Cp-}(CMe_2\text{-bridge})\text{-Ph})MII(ethylene)_2]^+$ (M = Ti, Zr, Hf) active catalysts: A density functional investigation of the influence of the metal on the cataly, *J. Am. Chem. Soc.*, 2004, **126**, 9059–9071.

90 F. Zaccaria, C. Ehm, P. H. M. Budzelaar and V. Busico, Accurate prediction of copolymerization statistics in molecular olefin polymerization catalysis: The role of entropic, electronic, and steric effects in catalyst comonomer affinity, *ACS Catal.*, 2017, **7**, 1512–1519.